TITLE

Artificial graphene nanoribbons: a testbed for topology and low-dimensional Dirac physics

AUTHORS

Daniel J. Trainer[1†], Srilok Srinivasan[1†], Brandon L. Fisher[1], Yuan Zhang[2], Constance R. Pfeiffer[1], Saw-Wai Hla[1,3], Pierre Darancet[1], Nathan P. Guisinger[1*]

AFFILIATIONS

[1]Center for Nanoscale Materials, Argonne National Laboratory, Lemont, Illinois 60439, United States.

[2]Department of Physics, Old Dominion University, Norfolk, Virginia 23529, United States.

[3]Department of Physics & Astronomy, Ohio University, Athens, Ohio 45701, United States.

*Correspondence to: nguisinger@anl.gov

[†]These authors contributed equally to this work

KEYWORDS: artificial lattices, graphene nanoribbons, topologically protected states, scanning tunneling microscopy, atomic-scale synthesis

ABSTRACT

We synthesize artificial graphene nanoribbons by positioning carbon monoxide molecules on a copper surface to confine its surface state electrons into artificial atoms positioned to emulate the low-energy electronic structure of graphene derivatives. We demonstrate that the dimensionality of artificial graphene can be reduced to one dimension with proper "edge" passivation, with the emergence of an effectively-gapped one-dimensional nanoribbon structure. These one dimensional structures show evidence of topological effects analogous to graphene nanoribbons. Guided by first-principles calculations, we spatially explore robust, zero-dimensional topological states by altering the topological invariants of quasi-one-dimensional artificial graphene nanostructures. The robustness and flexibility of our platform allows us to toggle the topological invariants between trivial and non-trivial on the same nanostructure. Ultimately, we spatially manipulate the states to understand fundamental coupling between adjacent topological states that are finely engineered and simulate complex Hamiltonians.

Topological insulators (TIs) are materials that belong to an electronic phase of matter that exhibit an insulating bulk coupled with protected and robust in-gap edge states [1-4]. Their electronic structure cannot be adiabatically deformed into topologically trivial insulators, making them more robust to defects and impurities, and are therefore of great interest to the spintronics and microelectronics communities [5, 6]. In addition, symmetry protected topological (SPT) states are critically important to the emerging field of quantum information science as they are predicted to host Majorana-fermion-like modes when proximity coupled to an s-wave superconductor [7-9]. A promising strategy to explore topological phases is to interface two structures with distinct topological character, consequently triggering the emergence of localized SPT states. This idea was pioneered by Su, Schrieffer and Heeger to describe the in-gap states that exist at domain boundaries in polyacetylene chains [10] and more recently has been exploited to engineer one-dimensional topological bands in graphene nanoribbons (GNRs) [11-13]. In the latter example, SPT states were produced at the junction between armchair GNR segments with varying topological character as defined by their Z2 invariant – the classification index that differentiates TIs (Z2 = 1) from trivial insulators (Z2 = 0) in gapped one-dimensional systems [14, 15]. The Z2 invariant of armchair GNRs can be tuned through their width, unit cell and edge termination thus offering a rich landscape for topological band engineering [12, 16, 17]. Navigating this landscape requires the ability to build GNRs of arbitrary shape with atomic scale precision on a one-atom-at-a-time basis, an ability that is generally not offered by bottom-up synthesis.

An alternative approach to exploring the band topology of graphene nanoribbons is through the platform of artificial lattices [18-20]. Demonstrated by Gomes, et al., artificial lattices of bulk graphene are created through the hexagonal arrangement of CO molecules on the surface of Cu (111) [21]. This is achieved when individual CO molecules are pushed along the surface with a

scanning tunneling microscopy (STM) tip to build arbitrary honeycomb structures one artificial atom at a time (Fig. 1A) [22]. The resulting molecular array repels the surface state electrons into a graphene-like honeycomb lattice, which demonstrates an analogous low-energy electronic dispersion as graphene yet with a reduced Fermi velocity.

In this work, we investigate the emergence and interplay between SPT states in topologically non-trivial artificial GNRs through the real-time manipulation of their geometries and consequently their Z2 invariants. Additionally, we control the coupling between adjacent states by adjusting their separation and show how it can be used to simulate complex Hamiltonians and quantum states.

Results and Discussion

Tailored artificial graphene nanostructures are constructed by first using first-principles calculations to identify a GNR which exhibits a non-trivial Z_2 invariant. The Z_2 invariant is determined from the origin independent part of the Zak phase as $Z_2 = \frac{1}{\pi}\int_{-\pi/d}^{\pi/d} dk\langle\psi_{n,k}|\partial_k|\psi_{n,k}\rangle \ mod\ 2$ (see supplemental section for further details). After identifying the topologically non-trivial nanoribbon geometries, corresponding atomic positions of CO molecules are mapped out and atomically manipulated on the Cu (111) surface such that the space in-between molecules reflect the GNR structure, as illustrated in Fig. 1B. These structures differ from artificial graphene in an analogous way to how GNRs differ from pristine graphene, namely that they are laterally confined. To this end, a "stitching" was developed where additional CO molecules were positioned around the edges of the hexagonal arrangement of COs (center and right column of Fig. 1b) to further confine the 2D electron gas to the inside of the nanoribbon.

The bulk-boundary correspondence dictates that boundary modes arise at the interface between a TI and trivial insulator, namely where there is a change in the Z_2 invariant [23]). We

demonstrate this effect at the edge of a topologically non-trivial N=9 armchair GNR (Z_2=1) and vacuum (Z_2=0) (Fig. 2A). The configuration of the atomic sites at the termination determines the nanoribbon unit cell, the origin of which determines the Z_2 invariant in one-dimension [12]. In Fig 2B, we demonstrate the switch between a topologically non-trivial and trivial nanoribbon by constructing an identical 9GNR but removing three artificial atoms from one zig-zag edge and adding them to the other side (Fig. 2B). The origin independent part of the Zak phase of the modified unit cell in Fig 2B (γ_2') is related to the original unit cell (γ_2) as $\gamma_2' = \gamma_2 - M\pi$, where M is the number of new (or old) lattice sites added (or removed), see supplemental section [17]. The topological class of the nanoribbon is changed from Z_2=1 to Z_2=0 since we move an odd number of sites effectively homogenizing its Z_2 invariant with the vacuum. To visualize the emergence of boundary modes along the non-trivial interface, we acquire simultaneous STM topographies and normalized differential conductance maps at -55meV of the topologically non-trivial (Fig. 2C) and trivial (Fig. 2D) nanoribbon. The SPT states that decorate the zig-zag edge of the non-trivial nanoribbon vanish when the structure becomes topologically trivial, corroborated by the local density of states (LDOS) maps calculated by tight-binding (TB) (bottom right panels). The LDOS at the zig-zag edge atoms are further investigated by acquiring dI/dV point spectroscopy (Fig. 2E). The spectrum on the non-trivial edge shows a resonance around -55meV that is not present on the trivial structure suggesting that it emerges from the spatial modulation of its topological character in agreement with the TB LDOS.

To distinguish topology from other mechanisms that could produce edge states we replace the vacuum with a 7GNR assembly. The resulting 7GNR/9GNR heterostructure contains artificial atoms along the interface with the same coordination as those in the bulk. The termination of the 7GNR segment, and hence the choice of unit cell, depends on whether the heterostructure is

symmetric (Fig. 3A) or asymmetric (Fig. 3B). The topological class of the symmetric and asymmetric unit cells is Z_2=0 and Z_2=1, respectively. These results are in agreement with Ref [12] and illustrate the relationship between band topology and nanoribbon unit-cell. To visualize the interface states, STM topographies and normalized differential conductance maps were acquired at -30meV over the artificial atoms of the non-trivial (Fig 3C) and trivial (Fig. 3D) interface. In agreement with the calculated LDOS maps (bottom panels), the conductance of the two nanoribbons is similar everywhere except for the interface. The dichotomy between the two interfaces is further exemplified in the magnified conductance maps of the non-trivial (Fig. 3E) and trivial (Fig. 3F) interfaces. Line profiles extracted from these maps over the first two rows of interfacial artificial atoms show the states present over the interface where the Z_2 invariant changes that vanish when both sides of the interface are topologically equivalent (Fig. 3G). Furthermore, the dI/dV point spectroscopy acquired on the artificial atom at the center of the interface in Figure 3E shows a resonance around -30meV that is absent in the spectrum acquired over the analogous atom in Figure 3F (Fig. 3H), in good agreement with the TB model.

Having established the presence of SPT states that arise from topological inequivalence, we demonstrate how these states and their couplings can be finely engineered to simulate complex Hamiltonians and quantum states. We consider a 9GNR/7GNR/9GNR heterostructure and examine the coupling between the SPT states by varying the lengths of its individual segments (Fig. 4A). This configuration results in 4 topological states ($\psi_{\{A,B,C,D\}}$) at the four interfaces between: (i) vacuum (Z_2=0) and 9GNR (Z_2=1), (ii) 9GNR (Z_2=1) and 7GNR (Z_2=0), (iii) 7GNR (Z_2=0) and 9GNR (Z_2=1) and (iv) 9GNR (Z_2=1) and vacuum (Z_2=0). The coupling between the adjacent states depends on their separation ($L_{\{AB,\ BC,\ CD\}}$). The TB wavefunctions of the 4 SPT states when they are well separated ($L \to \infty$) is shown in Fig. 4A.

To examine the range of coupling achievable between adjacent topological states and their robustness, we reduce the length of the middle segment L_{BC} separating B and C while increasing the length of the end segment L_{CD} separating C and D, thereby maintaining a constant total length (Fig. 4B). By moving state C towards a fixed state B and acquiring a line profile over the central resonance of the latter (Fig. 4C), the increased coupling between the two interface states leads to a decrease in the intensity of the peaks at both interfaces. As intensity is proportional to the square of the local components of the eigenstates, such a decrease in intensity demonstrates increased delocalization and the tunability of the wavefunction of the eigenstates resulting from the SPTs. Notably, the coupling between the interface state and end state results in a qualitatively distinct effect with measurable differences between the state B and C only occurring when $L_{CD} < 3$ unit cells (Fig. 4D). These trends are captured by the TB model (right panel in Fig. 4B and dashed lines in Fig. 4C & 4D).

The interplay between the four states and the effect of the different segment lengths can be understood by deriving a low-energy 4-state Hamiltonian in the form of a 1D chain with nearest neighbor interactions. As shown in supplementary information, the energy and hopping parameters are determined from TB modeling of the 9GNR/7GNR/9GNR geometry using projectors of states A, B, C, D derived from isolated interfaces and end state calculations. The wavefunctions associated with interface states B and C (end state A and D) are symmetric (anti-symmetric) with respect to the center of the ribbon, yielding $< \psi_A \mid H \mid \psi_B > = < \psi_C \mid H \mid \psi_D > = 0$, resulting in the low-energy behavior independent of L_{AB} and L_{CD} observed experimentally. The resulting behavior of the eigenstates of the low-energy Hamiltonian thus depends only on the strength of the interactions between interface states B and C. TB parametrization of the hopping terms yields a coupling of 15.6 meV for a one-unit-cell separation, decaying exponentially with separation at a

decay constant of 0.524/unit-cell, which reproduces the behavior observed in experiments (Fig. 4) and is further discussed in the supplemental section.

Conclusion

In summary, we have successfully synthesized artificial graphene nanoribbons at the atomic-scale by confining surface states of Cu(111). The geometric design of our artificial nanoribbons where chosen to exhibit topologically protected states and thereby confirm that these confined structures indeed have a bandgap. Our results offer a platform to explore and manipulate topological states in GNRs with atomic scale precision over their coupling. Ultimately, the interplay between adjacent SPT states demonstrated here provides fundamental insight into operations requiring the interaction between topological states, such as the braiding of Majorana pairs for topological quantum computation.

Experimental Section

The STM measurements were performed using an ultra-high vacuum (1.5 x 10-10 Torr) Createc microscope with an etched tungsten (W) tip operating at T = 5.3K. The tip was prepared by repeatedly crashing and pulsing into the Cu (111) surface and its quality verified by the Cu (111) surface state. The clean Cu (111) surface was prepared by repeated cycles of argon ion sputtering and annealing. The sample was placed on the scanner and allowed to cool to base temperature before dosing with 7.0 x 10-8 Torr of carbon monoxide (CO) molecules for 10 seconds. Spectroscopy of the symmetry protected topological (SPT) states were measured using a standard lock-in technique with a modulation voltage of 20mV and a modulation frequency of 1.125kHz.

FIGURES

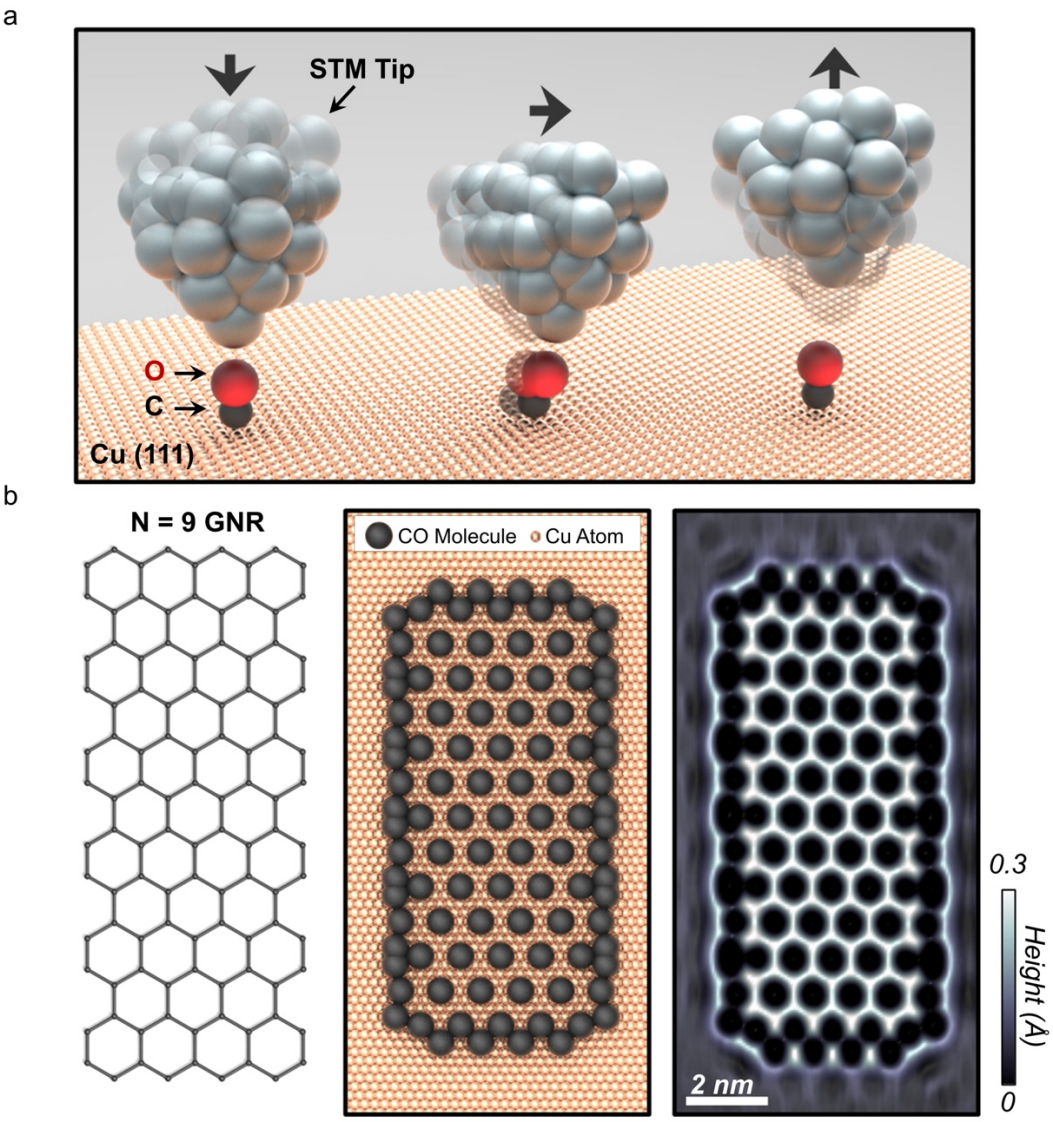

FIG. 1. Construction of artificial graphene nanoribbons. (a) Illustration of the atomic manipulation process used to move CO molecules on a Cu (111) surface. (b) (left panel) Identification of a non-trivial nanoribbon, (middle panel) mapping the corresponding CO positions on Cu (111) to obtain the analogous structure and (right panel) STM topography of the realized artificial GNR with $d_{CO\text{-}CO}$ = 1.0 nm (I_{set} = 0.5 nA, V_{set} = 750 mV).

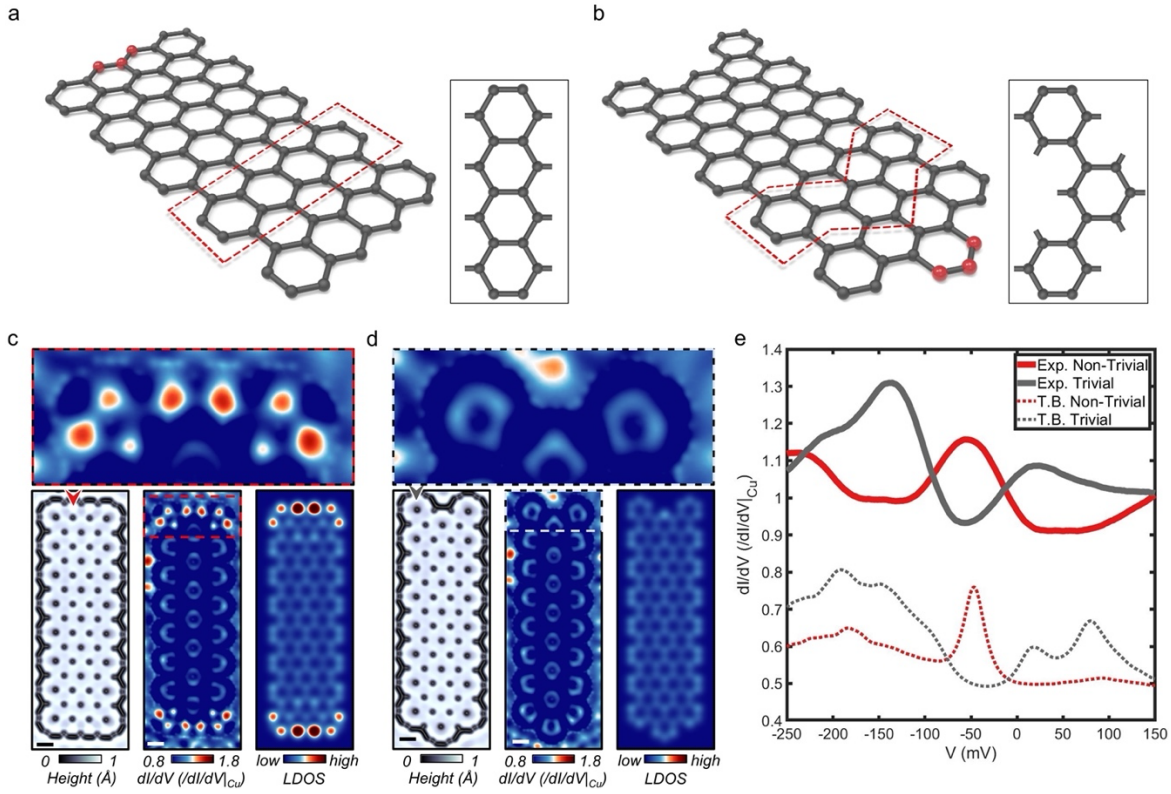

FIG. 2. Emergence of topological edge states in N = 9 artificial GNR. (a) Schematic of the topologically non-trivial N = 9GNR where the red dashed box encompasses the unit cell (inset). (b) Schematic of the trivial nanoribbon obtained by moving the three atoms highlighted in red in Fig.2a to the other edge of the nanoribbon. (c) and (d) (top panel) Magnified normalized differential conductance map acquired at -55meV taken on the zig-zag edge of the non-trivial and trivial nanoribbon, respectively. (bottom-left panel) STM topography, (bottom-middle panel) simultaneously acquired normalized differential conductance map and (bottom-right panel) calculated LDOS map of non-trivial and trivial structure, respectively (I_{set} = 1.0 nA, V_{set} = -55 mV, V_{mod} = 20mV). $d_{CO\text{-}CO}$= 2.0nm and scale bars represent 2nm. (e) dI/dV point spectroscopy taken on the positions marked on the STM topographies in Fig.2c and 2d (I_{set} = 0.5 nA, V_{set} = -500 mV, V_{mod} = 20mV).

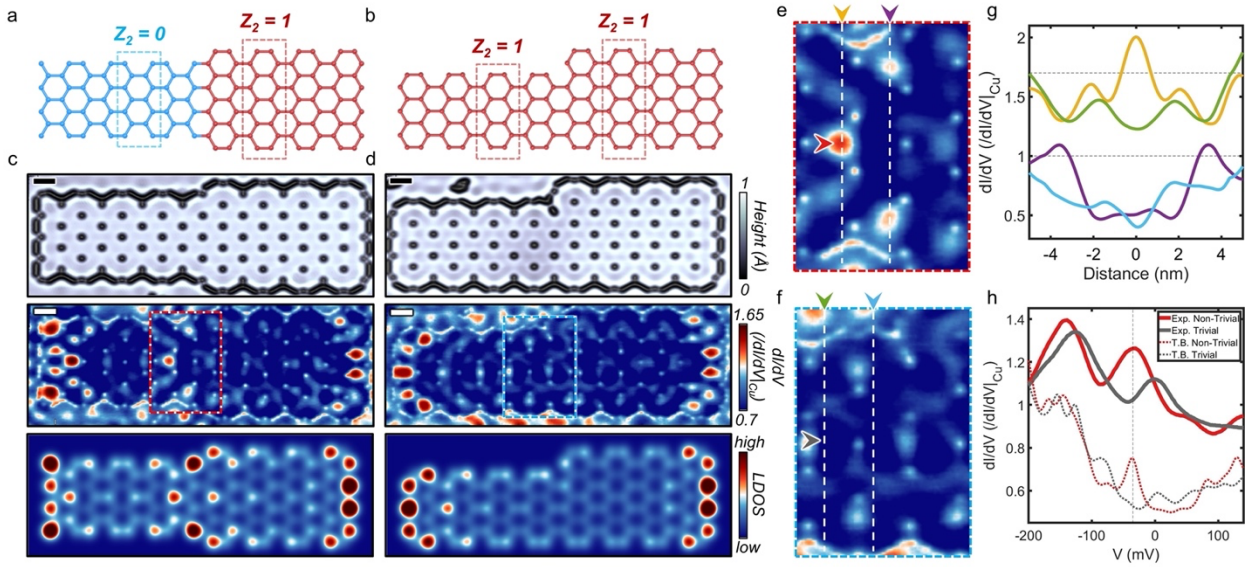

FIG. 3. Topological interface states in 7/9 heterostructures. (a) and (b) Illustrations of the topologically non-trivial and trivial heterostructure interfaces, respectively. (c) and (d) (top panel) STM topographies, (center panel) normalized differential conductance maps and (bottom panel) calculated TB LDOS maps of the artificial GNRs emulating the schematics from Fig.3a and 3b, respectively (I_{set} = 1.0 nA, V_{set} = -30 mV, V_{mod} = 20mV). Scale bars represent 2nm. (e) and (f) Magnification of the interfaces outlined by the dashed boxes in Fig.3c and 3d, respectively. (g) Cross sectional line cuts of the differential conductance maps along the dashed lines in Fig.3e and 3f. (h) dI/dV point spectroscopy acquired on the horizontal indicators in Fig.3e and 3f (I_{set} = 0.5 nA, V_{set} = -500 mV, V_{mod} = 20mV).

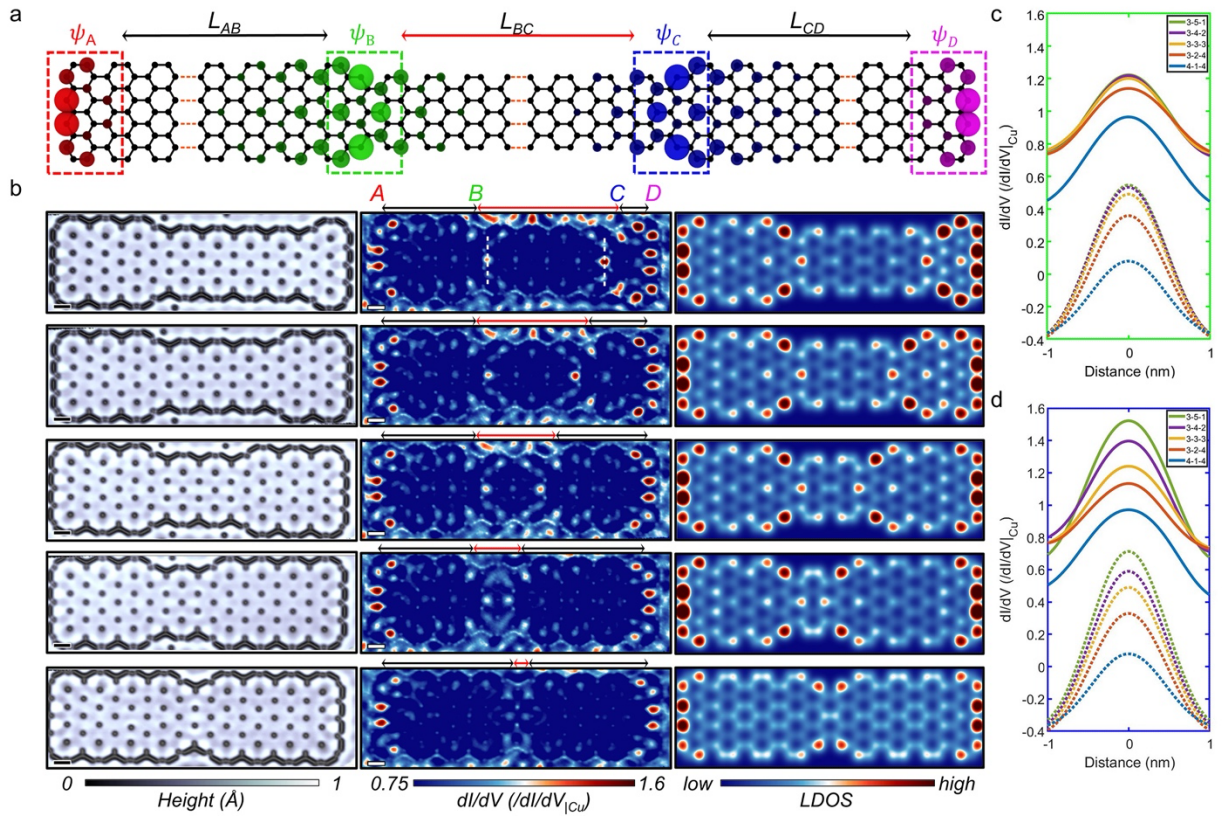

FIG. 4. Interplay between SPT states. (a) Wavefunctions of 4 SPT states in a 9GNR/7GNR/9GNR heterostructure. The distances between the states are represented as L_{AB}, L_{BC} and L_{CD}, respectively. (b) A series of (left column) STM topographies, (middle column) normalized differential conductance maps and (right column) TB LDOS maps of an artificial GNR while varying the separation between states (I_{set} = 1.0nA, V_{set} = -30mV, V_{mod} = 20mV). (c) and (d) Line profiles taken over the central states at sites B and C, respectively. Scale bars represent 2nm. These line profiles are represented as the dashed white lines in the conductance maps (solid lines) from the middle column of Fig.4b and the TB LDOS maps (dashed lines) from the right column of Fig.4b.

TOC

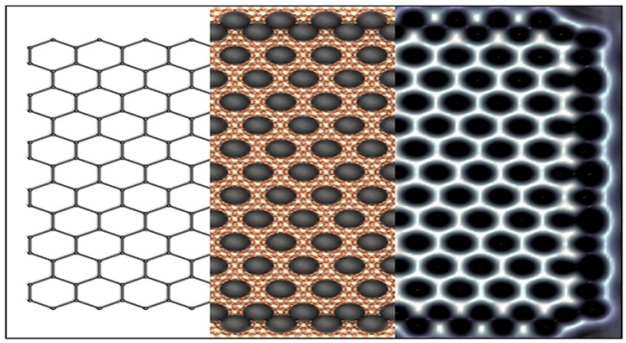

ASSOCIATED CONTENT

Supporting Information

The Supporting Information is available online at: XXX

Section 1: Scanning Tunneling Microscopy and Spectroscopy

Section 2: Muffin Tin Calculations

Section 3: Tight Binding Calculations

Section 4: Parameterization of tight binding parameters

Section 5: Topological classification

Section 6: Manipulating topology by changing the unit cell

Section 7: Effective Hamiltonian of topological states

Preprint Submission: Daniel J. Trainer, Srilok Srinivasan1, Brandon L. Fisher, Yuan Zhang, Constance R. Pfeiffer, Saw-Wai Hla, Pierre Darancet, Nathan P. Guisinger, “Artificial graphene

nanoribbons: a testbed for topology and low-dimensional Dirac physics", 2021, 2104.11334, arXiv, https://arxiv.org/abs/2104.11334. (accessed April 26, 2021).

AUTHOR INFORMATION

Corresponding Author

Nathan P. Guisinger

*Correspondence to: nguisinger@anl.gov

Author contributions: DJT, SS, PD, and NPG led the conception, design, acquisition, and analysis of this research along with drafting this manuscript. BLF and CRP provided logistical support for data acquisition. YZ contributed in atomic manipulation and spectroscopy in data acquisition. SWH provided critical guidance and support.

Funding: U.S. Department of Energy, Office of Science, Basic Energy Science

Competing interests: Authors declare no competing interests.

ACKNOWLEDGMENT

This work was performed at the Center for Nanoscale Materials, a U.S. Department of Energy Office of Science User Facility, and supported by the U.S. Department of Energy, Office of Science, under Contract No. DE-AC02-06CH11357. This material is based upon work supported by Laboratory Directed Research and Development (LDRD) funding from Argonne National Laboratory, provided by the Director, Office of Science, of the U.S. Department of Energy under Contract No. DE-AC02-06CH11357.

REFERENCES

1. Fu, L.; Kane, C. L. Topological insulators with inversion symmetry. *Physical Review B* **2007,** *76*, 045302.
2. Hasan, M. Z.; Kane, C. L. Colloquium: Topological insulators. *Reviews of Modern Physics* **2010**, *82*, 3045-3067.
3. Bernevig, B. A.; Hughes, T. L.; Zhang, S.-C. Quantum spin hall effect and topological phase transition in HgTe quantum wells. *Science* **2006**, *314*, 1757-1761.
4. Xu, C.; Moore, J. E. Stability of the quantum spin Hall effect: Effects of interactions, disorder, and Z_2 topology. *Physical Review B* **2006**, *73*, 045322.
5. Fu, L. Topological crystalline insulators. *Physical Review Letters* **2011***, 106*, 106802.
6. König, M.; Wiedmann, S.; Brüne, C.; Roth, A.; Buhmann, H.; Molenkamp, L. W.; Qi, X.-L.; Zhang S.- H. Quantum Spin Hall Insulator State in HgTe Quantum Wells. *Science* **2007**, *318*, 766-770.
7. Fu, L.; Kane, C. L. Superconducting proximity effect and Majorana Fermions at the surface of a topological insulator. *Physical Review Letters* **2008**, *100*, 096407.
8. Jäck, B.; Xie, Y.; Li, J.; Jeon, S.; Bernevig, B. A.; Yazdani, A. Observation of a Majorana zero mode in a topologically protected edge channel. *Science* **2019**, *364*, 1255-1259.
9. Nadj-Perge, S.; Drozdov, I. K.; Li, J.; Chen, H.; Jeon, S.; Seo, J.; Macdonald, A. H.; Bernevig, B. A.; Yazdani, A. Observation of Majoran fermions in ferromagnetic atomic chains on a superconductor. *Science* **2014**, *346*, 602-607.
10. Su, W. P.; Schrieffer, J. R.; Heeger, A. J. Solitons in polyacetylene. *Physical Review Letters* **1979**, *42*, 1698-1701.

11. Rizzo, D. J.; Veber, G.; Cao, T.; Bronner, C.; Chen, T.; Zhao, F.; Rogriguez, H.; Louie, S. G.; Crommie, M. F.; Fischer, F. R. Topological band engineering of graphene nanoribbons. *Nature* **2018**, *560*, 204-208.

12. Cao, T.; Zhao, F.; Louie, S. G. Topological Phases in Graphene Nanoribbons: Junction States, Spin Centers, and Quantum Spin Chains. *Physical Review Letters* **2017**, *119*, 076401.

13. Gröning, O.; Wang, S.; Yao, X.; Pignedoli, C. A.; Barin, G. B.; Daniels, C.; Cupo, A.; Meunier, V.; Feng, X.; Narita, A.; Müllen, K.; Ruffieux, P.; Fasel, R. Engineering of robust topological quantum phases in graphene nanoribbons. *Nature* **2018**, *560*, 209-213.

14. Kane, C. L.; Mele, E. J. Z2 Topological Order and the Quantum Spin Hall Effect. *Physical Review Letters* **2005**, *95*, 146802.

15. Kaufmann, R. M.; Li, D.; Wehefritz-Kaufmann, B. Notes on topological insulators. *Reviews in Mathematical Physics* **2016**, *28*, 1630003.

16. Lee, Y.-L.; Zhao, F.; Cao, T.; Ihm, J.; Louie, S. G. Topological Phases in Cove-Edged and Chevron Graphene Nanoribbons: Geometric Structures, Z2 Invariants, and Junction States. *Nano Letters* **2018**, *18*, 7247-7253.

17. Lin, K.-S.; Chou, M.-Y. Topological Properties of Gapped Graphene Nanoribbons with Spatial Symmetries. *Nano Letters* **2018**, *18*, 7254-7260.

18. Yan, L.; Liljeroth, P. Engineered electronic states in atomically precise artificial lattices and graphene nanoribbons. *Advances in Physics: X* **2019**, *4*, 1651672.

19. Gardenier, T. S.; van de Broeke, J. J.; Moes, J. R.; Swart, I.; Delerue, C.; Slot, M. R.; Simth, M.; Vanmaekelbergh, D. p Orbital Flat Band and Dirac Cone in the Electronic Honeycomb Lattice. *ACS Nano* **2020**, *14*, 13638-13644.

20. Kempkes, S. N.; Slot, M. R.; van de Broeke, J. J.; Capiod, P.; Benalcazar, W. A.; Vanmaekelbergh, D.; Bercious, D.; Swart, I.; Smith, C. M. Robust zero-energy modes in an electronic higher-order topological insulator. *Nature Materials* **2019**, *18*, 1292-1297.

21. Gomes, K. K.; Mar, W.; Ko, W.; Guinea, F.; Manoharan, H. C. Designer Dirac fermions and topological phases in molecular graphene. *Nature* **2012**, *483*, 306-310.

22. Hla, S. W. Atom-by-atom assembly. *Reports on Progress in Physics* **2014**, *77*, 056502.

23. Rhim, J.-W.; Behrends, J.; Bardarson, J. H. Bulk-boundary correspondence from the intercellular Zak phase. *Physical Review B* **2017**, *95*, 035421.